CellPress

# Supplemental figures

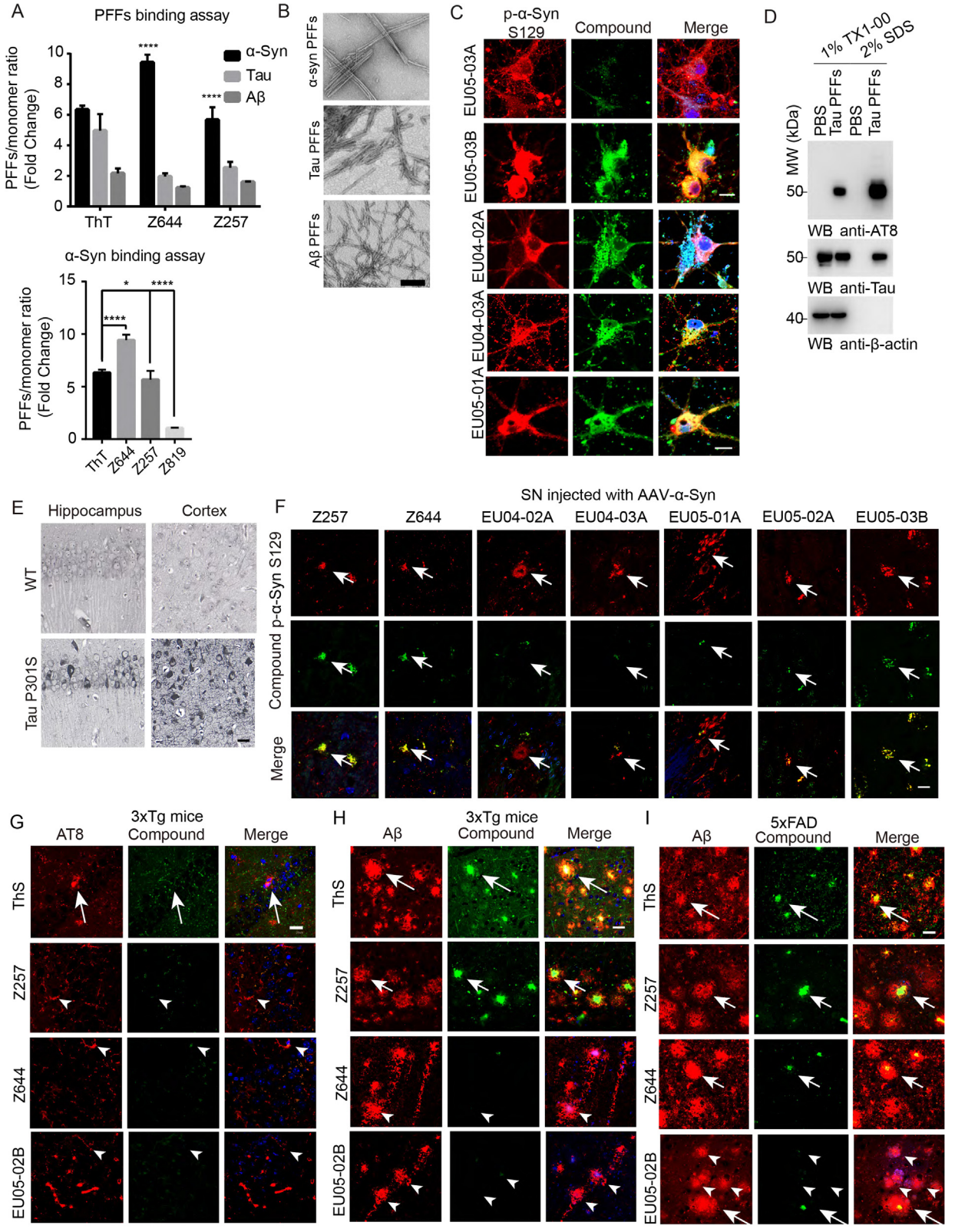


*(legend on next page)*

**Figure S1. Selectivity of the candidate chemicals to α-Syn aggregates, related to Figure 1**

(A) Chemical binding ratio with preformed fibers (PFFs) and monomers of α-Syn, Tau, or Aβ was detected by a light scattering assay (ThT: Ex 440 nm, Em 485 nm; Z644 Ex 420 nm, Em 525 nm; Z257 Ex 423 nm, Em 540 nm). Upper, Z644 and Z257 showed stronger binding affinity with α-Syn. Lower, binding affinities of chemicals with α-Syn, *$p < 0.05$, ****$p < 0.0001$, two-way ANOVA. Error bars represent the mean ± SEM. Data are representative of 3 independent experiments.

(B) TEM of α-synuclein, Tau, and Aβ PFFs.

(C) Confocal fluorescence images of neurons with α-Syn aggregates. Neurons were infected with AAV-α-Syn at DIV 7 and transduced with α-Syn PFFs at DIV 12 to induce α-Syn aggregation. The samples were immune-stained with an antibody against p-α-Syn S129 (pseudocolors were converted to red) to detect α-Syn aggregates and then stained with candidate chemicals (0.1 μM). Scale bars, 10 μm.

(D) Sequential extraction shows that Tau PFFs triggered the formation of insoluble Tau aggregates in primary neurons.

(E) Silver staining of brain sections from the hippocampus and cortex of Tau P301S mice.

(F) Double staining of α-Syn aggregates in mouse SN injected with AAV-α-Syn A53T with candidate chemicals and p-α-Syn S129 antibody. All chemicals except EU04-02A sensitively captured α-Syn aggregation in the SN area (arrows). Scale bars, 20 μm.

(G and H) Double staining of Aβ plaques and NFTs in 14-month-old 3xTg mouse cortex with candidate chemicals and Aβ antibody (6E10) or AT8. Z257 stained senile plaques (arrowheads) in slices, but Z644 barely recognized Aβ plaques or NFTs (arrowheads). Scale bars, 20 μm.

(I) Double staining of Aβ plaques in the cortex of 12-month-old 5xFAD mice with candidate chemicals or ThS and Aβ (6E10). Scale bars, 20 μm.

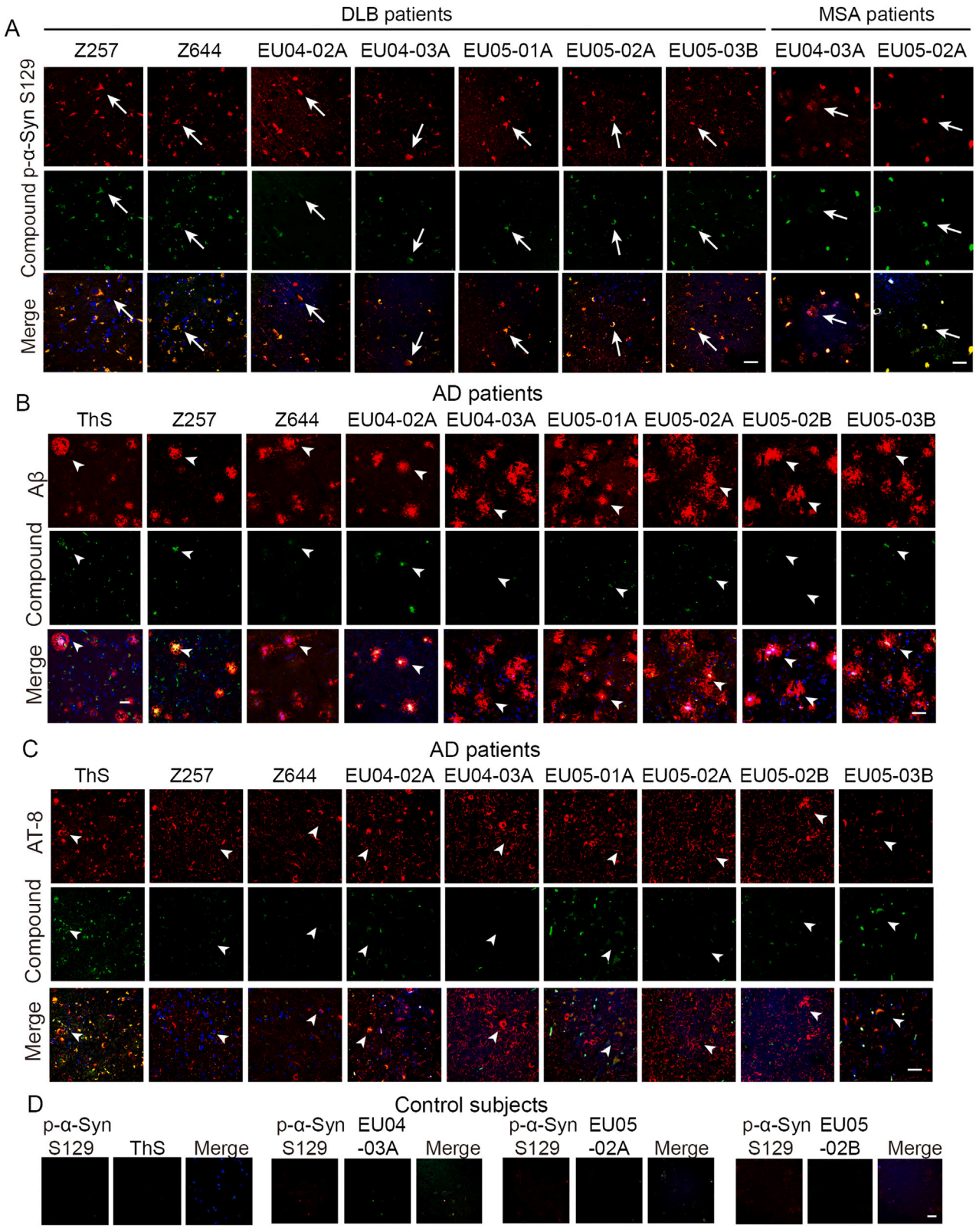


*(legend on next page)*

**Figure S2. EU05-02B selectively interacts with Lewy bodies in PD patients, related to Figure 1**

(A) Double staining of α-Syn aggregates in the cortex of DLB patients and SN of MSA patients with candidate chemicals and p-α-Syn S129 antibody. Scale bars, 20 μm. All chemicals captured α-Syn aggregates (arrows). Scale bars, 20 μm.

(B) Double staining of senile plaques in the AD cortex with candidate chemicals or ThS and Aβ antibodies (6E10). ThS detected senile plaques in brain slices (arrows). Scale bars, 20 μm.

(C) Double staining of NFTs in the AD cortex with candidate chemicals or ThS and p-Tau antibody (AT8). Scale bars, 20 μm.

(D) Double staining of α-Syn aggregates in the control cortex with candidate chemicals and p-α-Syn S129 antibody. Scale bars, 20 μm.

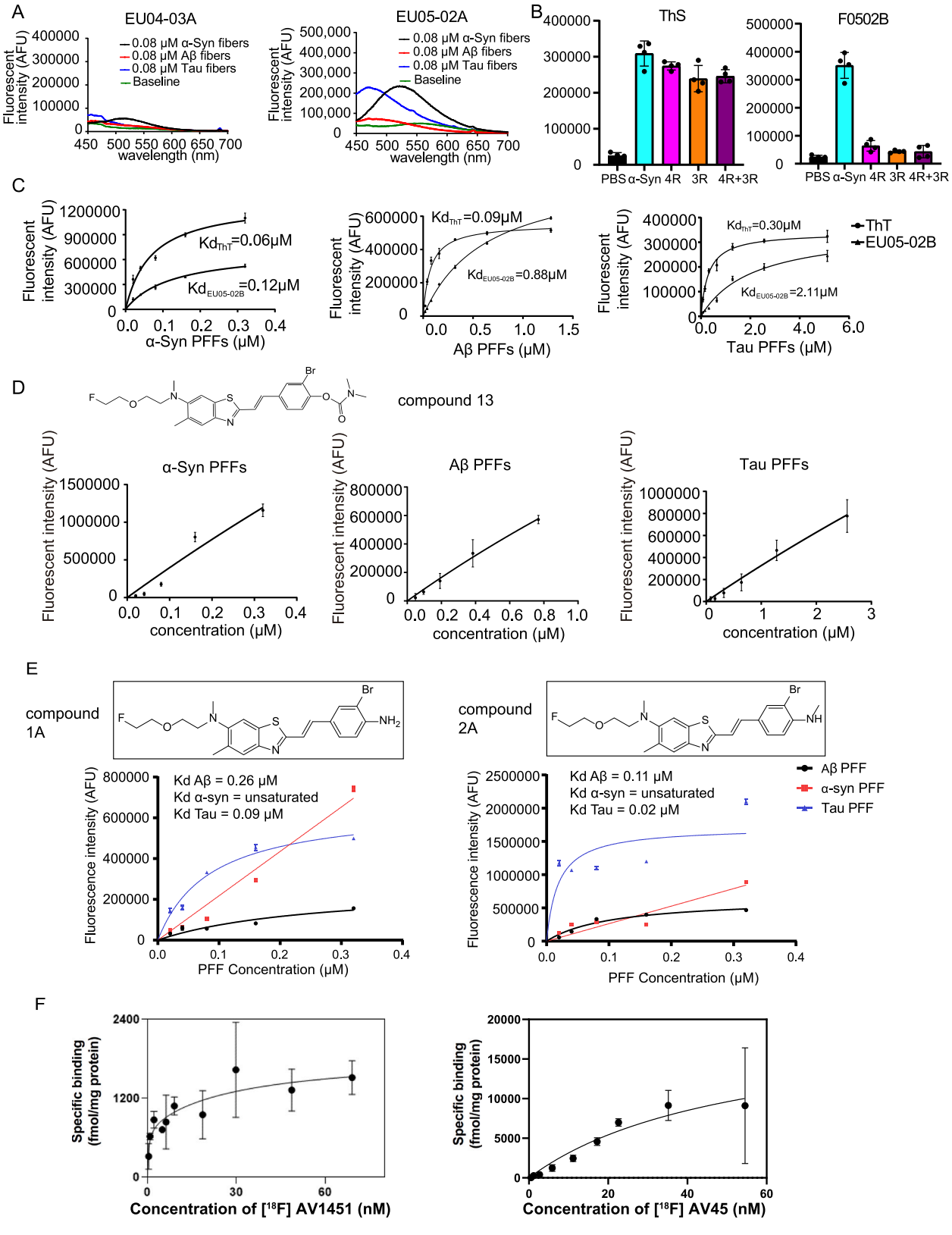


(legend on next page)

**Figure S3. EU05-02B and F0502B specifically interact with α-Syn fibrils, related to Figure 2**

(A) Fluorescent binding study of EU04-03A and EU05-02A with α-Syn, Tau, and Aβ PFFs.

(B) The binding assays of F0502B to 3R, 4R, and 3R-4R mixed Tau fibrils. Data points represent the mean ± SD. Similar results were obtained in more than three independent experiments for saturation binding studies.

(C) Quantification of binding affinities demonstrated that ThT and EU05-02B bound to α-Syn, Aβ, and Tau PFFs. The binding affinities of ThT and EU05-02B to PFFs were determined in saturation binding studies. The determined $K_d$ values of α-Syn, Aβ, and Tau PFFs are shown in the graphs. Data points represent the mean ± SD.

(D and E) Substitution of the hydroxy group abolishes its binding to α-synuclein fibrils. (D) Saturation binding studies of compound 13. Data points represent the mean ± SD. Similar results were obtained in more than three independent experiments for saturation binding studies. (E) Saturation binding studies of amino-compounds 1A and methylamino-2A. Data points represent the mean ± SD. Similar results were obtained in more than three independent experiments for saturation binding studies.

(F) Validation of Aβ plaques and Tau tangles in AD brain lysates. The $K_d$ and $B_{max}$ were 0.4 nM and 0.77 pmol/mg for Tau tracer [$^{18}$F] AV1451 and 52.8 nM and 19.7 pmol/mg for Aβ tracer [$^{18}$F] AV45, respectively, indicating that the AD samples contained abundant Tau tangles and dense-core plaques. Data points represent the mean ± SD. Similar results were obtained in more than three independent experiments.

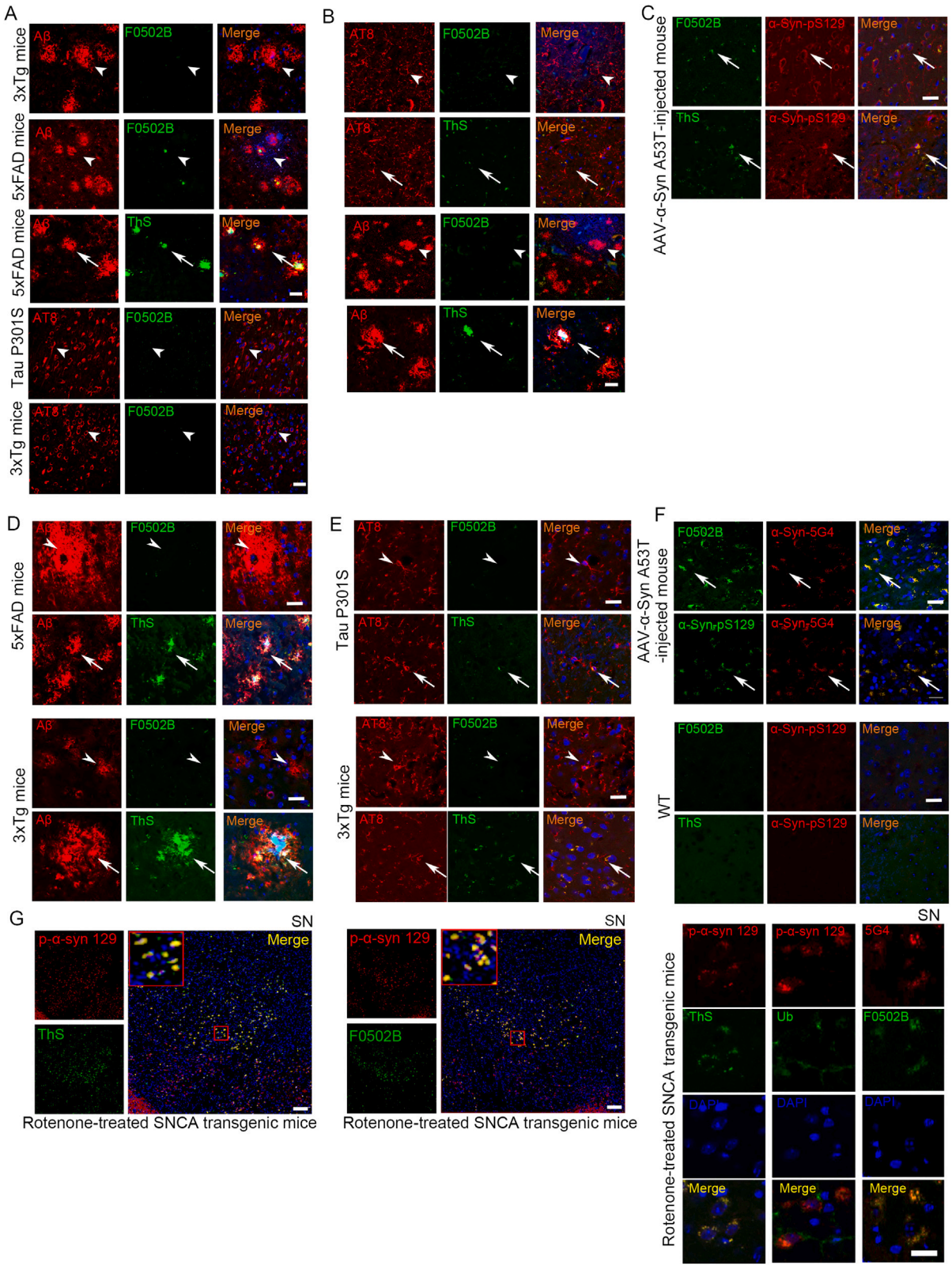


*(legend on next page)*

**Figure S4. F0502B selectively interacts with α-Syn aggregates, related to Figure 2**

(A) Double staining of Aβ plaques and NFTs in AD transgenic mice with F0502B or ThS and Aβ antibody (6E10) or AT8 antibody. The brain slices were from 14-month-old 3xTg mouse cortex, 6-month-old Tau P301S mouse cortex, and 12-month-old 5xFAD mouse cortex. Scale bars, 20 μm.

(B) Double staining of Aβ plaques or NFTs in the AD patient cortex with F0502B and Aβ antibody (6E10) or AT8. Scale bars, 20 μm.

(C) Confocal images of F0502B/ThS (green), p-α-Syn S129 (red), and 4′,6-Diamidino-2-phenylindole (DAPI) (blue) in the SN of AAV-α-Syn A53T-injected mice. Scale bars, 20 μm.

(D–F) 8-month-old wild-type, 5xFAD, Tau P301S, 3xTg, and AAV-α-Syn A53T-injected mice were injected with F0502B via the vena caudalis at 2 mg/kg. Brain sections were prepared 2 h after injection. (D) Confocal analysis of F0502B/ThS (green), Aβ (red), and DAPI (blue) localization in the cortex of 5xFAD and 3xTg mice. Scale bars, 20 μm.

(E) Confocal analysis of F0502B/ThS (green), AT8 (red), and DAPI (blue) in the frontal cortex of Tau P301S and 3xTg mice. Arrows show positive co-localization signals. Scale bars, 20 μm.

(F) Double fluorescence staining of intraneuronal α-Syn aggregates in the SN of AAV-α-Syn A53T-injected mice and control mice with F0502B, anti-pS129, or aggregated α-Syn antibody (5G4). Scale bars, 20 μm.

(G) F0502B detects α-Syn aggregates in rotenone-treated SNCA Tg mice. Left and middle, immunofluorescence co-staining of p-α-Syn 129 (red), DAPI (blue) and ThS/F0502B (green) in the SN of the rotenone-treated SNCA Tg mice. Scale bars, 100 μm. Right, co-staining of p-α-Syn 129 (red)/ThS (green), p-α-Syn 129 (red)/ubiquitin (Ub, green), and 5G4 (red)/F0502B (green) for rotenone-treated SNCA Tg mice. Scale bars, 20 μm.

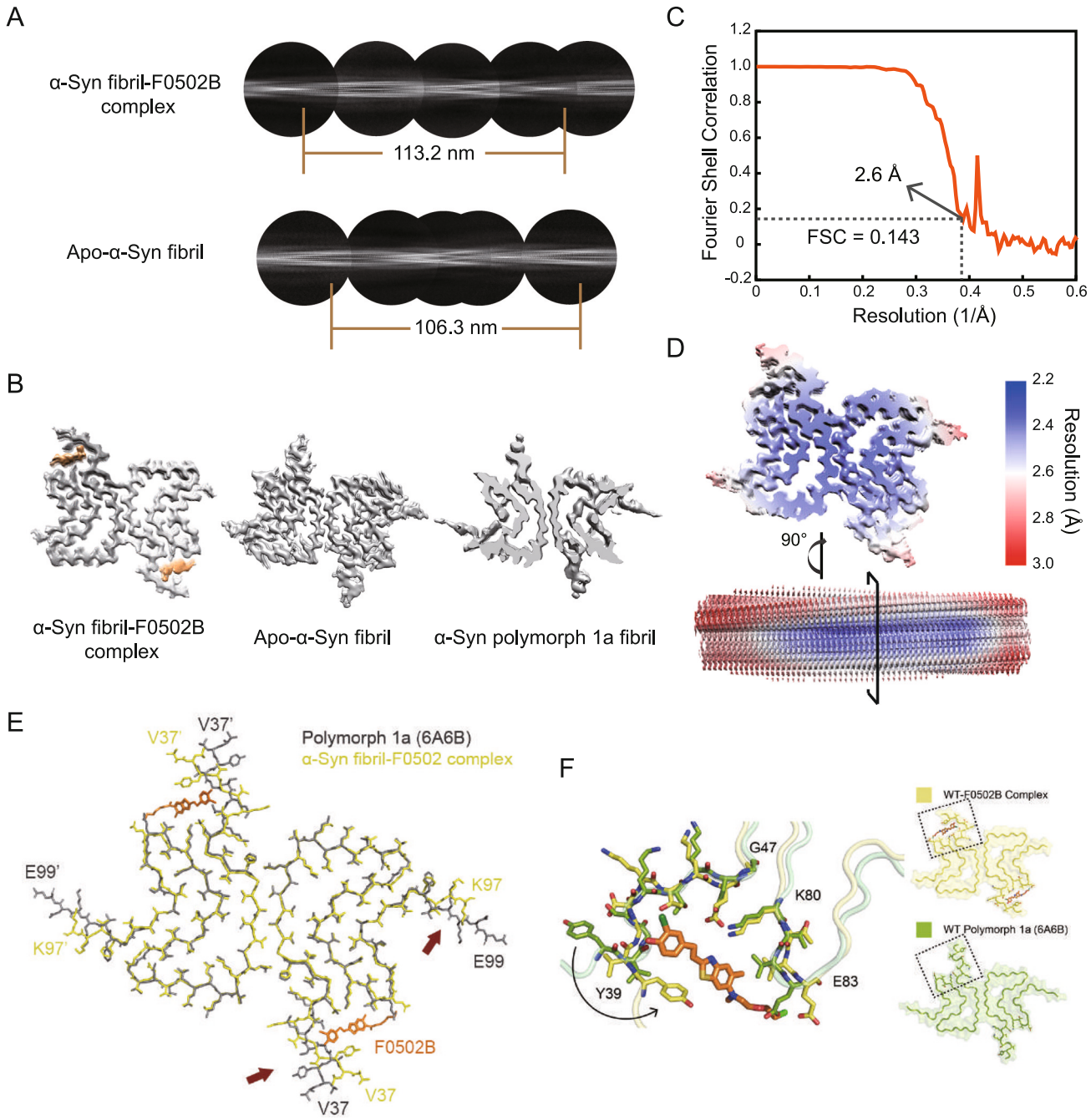


**Figure S5. Helical reconstruction of the α-Syn fibril-F0502B complex and the structure comparison with apo-α-Syn fibril, related to Figure 5**

(A) 2D class averages of the α-Syn fibril-F0502B complex and apo-α-Syn fibril. The lengths of half pitch are indicated.

(B) 3D density maps of the α-Syn fibril-F0502B complex, apo-α-Syn fibril, and α-Syn polymorph 1a (available from PDB: 6A6B, EMDB: EMD-6988).

(C) Overall resolution estimation of the cryo-EM density map of α-Syn fibril-F0502B complex. Gold standard Fourier shell correction (FSC) curves of two independently refined half-maps.

(D) Estimation of local resolution of the recombinant density map of α-Syn fibril-F0502B complex.

(E) Alignment of α-Syn fibril structures: α-Syn fibril-F0502B complex versus polymorph 1a (PDB: 6A6B). The two structures are nearly identical with an RMSD of 0.632 Å. Main discrepancies lie in the termini where the amino acid chains are relatively flexible. The red arrows indicate termini of α-Syn in the fibril core.

(F) Zoom-in view of the F0502B binding cavity shown in sticks. Structural alignment on the basis of similarities: α-Syn fibril-F0502B complex versus polymorph 1a, RMSD of 0.557 Å over 49 C-α atoms (global alignment), and 1.132 Å over 12 C-α atoms (pocket alignment).

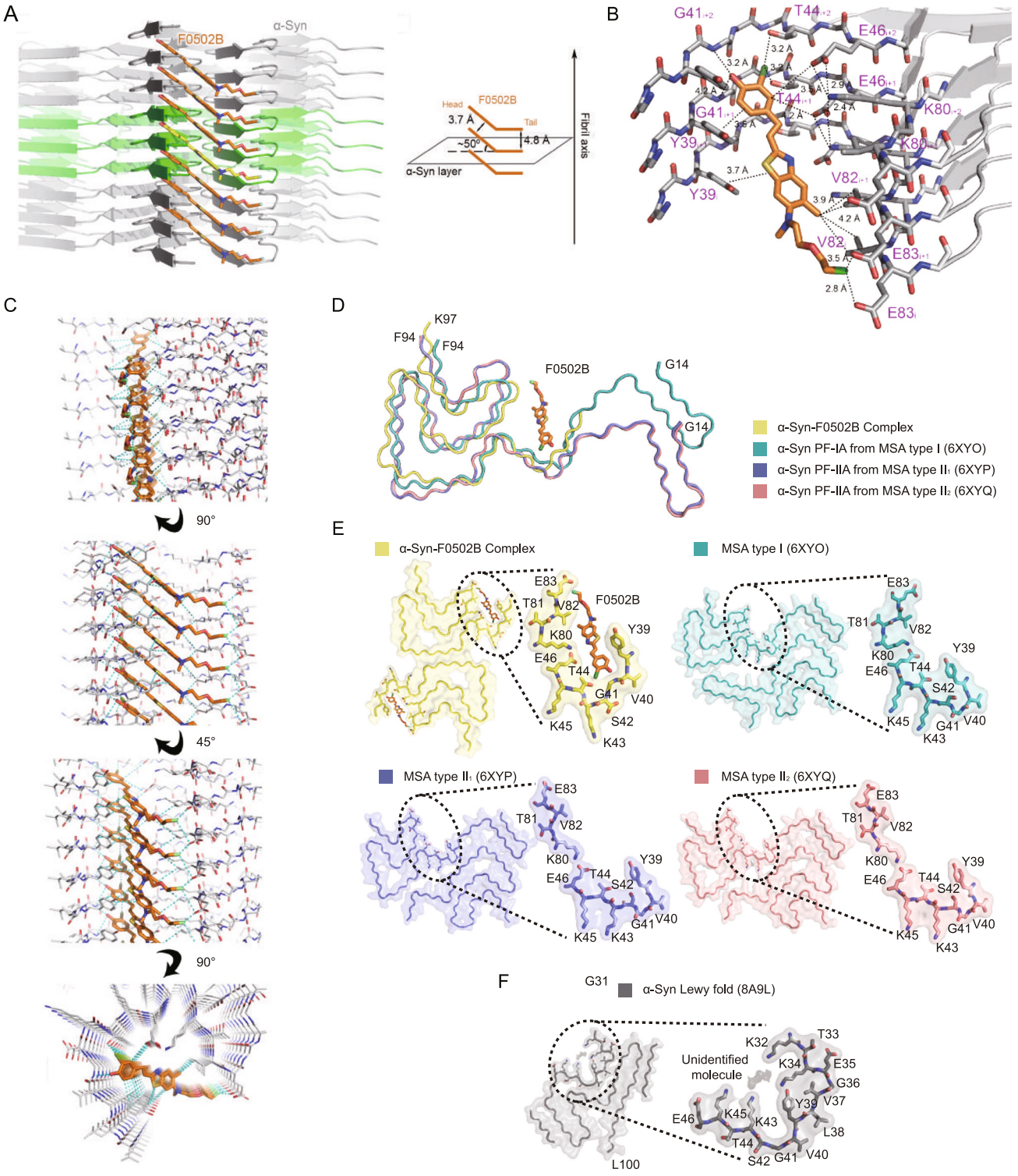


**Figure S6. Inter-ligand and ligand-α-Syn interactions of F0502B, related to Figure 6**

(A) The packing geometry of F0502B molecules along the fibril axis. Overview of the orientation of the aromatic plane, the fluoro tail, and the plane of α-Syn layers. Nine layers of α-Syn molecules along the fibril are shown in cartoon. The middle 3 layers are highlighted in green. F0502B binds over the middle 3 layers of α-Syn and is highlighted in yellow. Detailed distances and angles are indicated on the right.

(B) Overview of the interactions between F0502B and α-Syn fibrils. Pocket residues are in stick representation colored by heteroatom. F0502B is shown in orange. Detailed interaction distances are labeled.

*(legend continued on next page)*

(C) Views of the interaction network of F0502B and the α-Syn fibril. The fibril-ligand complex structure is shown in stick representation with α-Syn in gray and F0502B in orange. The interactions between the fibril and ligand are indicated by cyan dashed lines.
(D) Structural comparison of the α-Syn fibril-F0502B complex with *ex vivo* α-Syn fibrils from MSA and PD/DLB. Overlay of the α-Syn monomeric structures in the fibrils including α-Syn fibril-F0502B (yellow), type I filaments from MSA (cyan, PDB: 6XYO), type $II_1$ filaments from MSA (blue, PDB: 6XYP), and type $II_2$ filaments from MSA (red, PDB: 6XYQ). Structural alignment on the basis of similarities: α-Syn fibril-F0502B complex versus MSA type I, RMSD of 2.288 Å over 53 C-α atoms (global alignment), and 1.809 Å over 12 C-α atoms (pocket alignment); α-Syn fibril-F0502B complex versus MSA type $II_1$, RMSD of 4.537 Å over 58 C-α atoms (global alignment), and 4.066 Å over 13 C-α atoms (pocket alignment); α-Syn fibril-F0502B complex versus MSA type $II_2$, RMSD of 4.528 Å over 58 C-α atoms (global alignment), and 4.127 Å over 13 C-α atoms (pocket alignment).
(E) Overall structures of the α-Syn fibrils shown in (D). Putative ligand-binding cavities are depicted by dashed circles and zoomed-in with residues shown in sticks. F, The structure of α-Syn fibrils Lewy fold (PDB: 8A9L). Putative ligand-binding cavity is zoomed-in with residues shown in sticks. An unidentified molecule is shown with density.

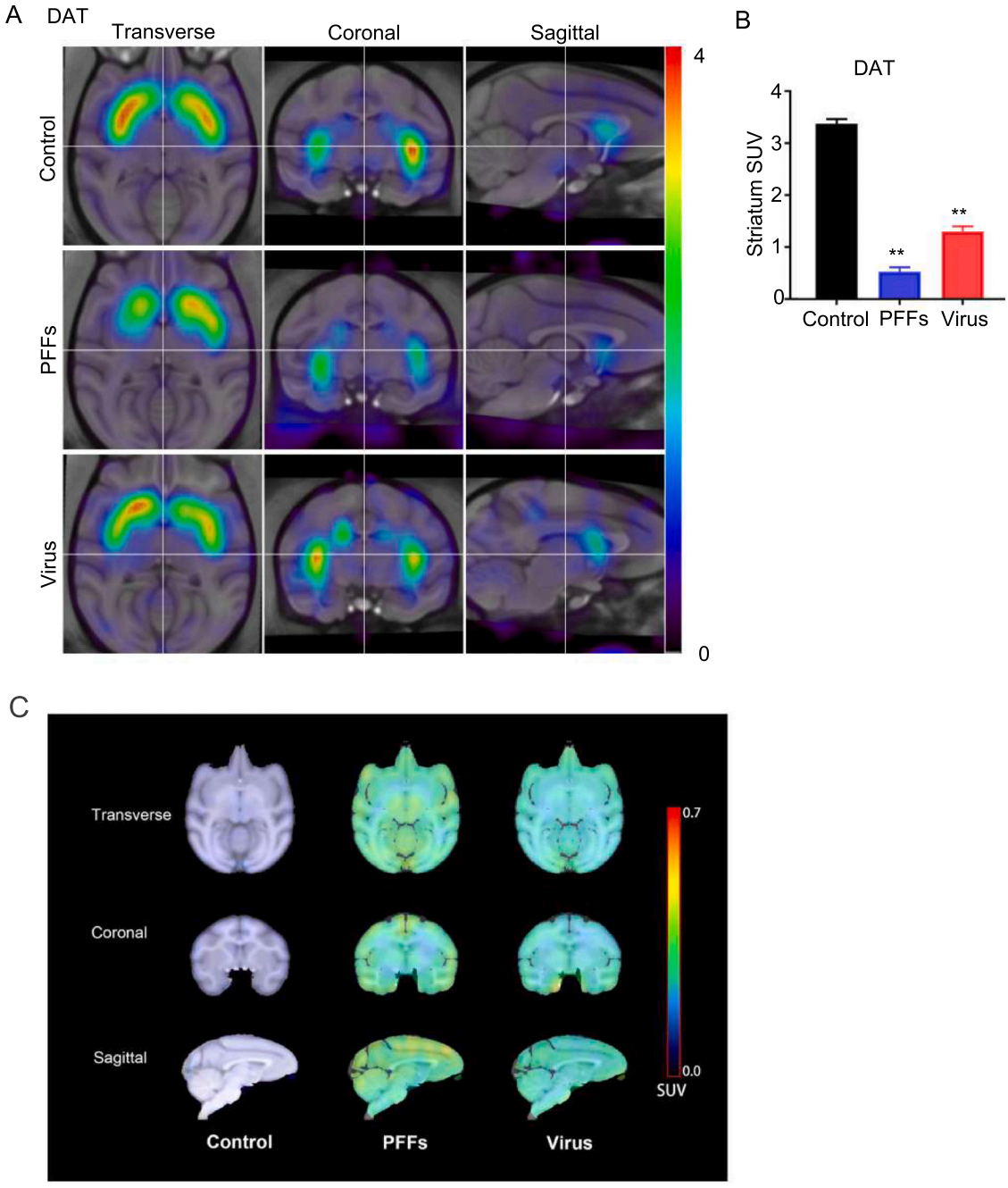


**Figure S7. PET imaging of DAT with [$^{11}$C]-CFT and [$^{18}$F]-F0502B in non-human primate PD models, related to Figure 7**

(A) [$^{11}$C]-CFT visualizes dopamine transporter (DAT) in the brains of macaques injected with α-Syn PFFs, AAV-α-Syn A53T, and control virus. PET images in each row represent the standardized uptake value (percentage of injected dose per cubic centimeter (%ID/cc) × body weight) averaged over a 10 period at 30 min post-injection, co-registered to MRI, from left to right showing axial, coronal and sagittal views.

(B) The brain uptake kinetics of [$^{11}$C]-CFT. The macaques were i.v. injected with [$^{11}$C]-CFT. The dynamic PET activity of the striatum-VOI (volume-of-interest) in these 3 strains of macaques was recorded at 30 min post-injection. Values are the standardized uptake value (mean ± SD, **$p < 0.01$, $n = 3$, two-way ANOVA).

(C) [$^{18}$F]-F0502B detects signals in the brains of macaques injected with α-Syn PFFs and AAV-α-Syn A53T but not in the brains of control macaques. PET images in each row represent the standardized uptake value (percentage of injected dose per cubic centimeter (%ID/cc) × body weight) averaged over a 30 min period at 60 min post-injection, co-registered to an MRI imaging template edited out the extracerebral tissues, from left to right showing axial, coronal, and sagittal views.